C-H bonds in Carbon Nanotubes as an Energy Carrier

Final report 2012

Investigators

Principal Investigators: Anders Nilsson (SSRL), Bruce Clemens (Materials Science and Engineering), Hongjie Dai (Chemistry)
Hirohito Ogasawara (staff scientist, SSRL), Daniel Friebel (staff scientist, SSRL), Srivats Rajasekaran (PhD student, Materials Science and Engineering), Liying Jiao (postdoc, Chemistry), Cara Beasley (Graduated (May 2012), Chemistry), Ranadeep Bhowmick (Graduated (May 2012), Material Science and Engineering)

Abstract

The main goal of this work was to study the hydrogen interactions with carbon nanostructures (graphene grown on Pt(111), and carbon nanotube (CNT)/Pt composites) in lieu towards finding answers related to two bigger questions – (a) hydrogen storage possibility in carbon nanostructures and (b) band gap opening in graphene (for device applications).

X-ray spectroscopy was used as the main experimental probe since it provides for an atom specific probe of the electronic structure pertaining to the carbon atoms. We utilize the following x-ray spectroscopic techniques – X-ray photoelectron spectroscopy (XPS), X-ray absorption spectroscopy (XAS), and X-ray emission spectroscopy (XES) along with other typical surface science techniques to probe the chemical environment and the electronic structure of the carbon atoms while they interact with hydrogen.

For hydrogen storage applications, one would need a material that would undergo loading/unloading at conditions close to ambient conditions. In other words, the material would have the adsorption and desorption energies of hydrogen to be energetically neutral (i.e. close to zero) such that no energy loss would occur during the loading/unloading process. In this work, we have successfully demonstrated two routes towards reducing the kinetic barrier involved in the process of (de-)hydrogenation. One involved hydrogenation of CNT/Pt composites at near ambient conditions (~8.25 atm of hydrogen gas at room temperature) exploiting the concept of "spillover" of H atoms from H_2 molecules dissociated on the Pt catalyst. The other experiment involved the reduction in the C-H desorption barriers for graphene grown on Pt substrate, through modulation of the electronic structure of the Pt substrate through a subsurface layer of Co atoms forming a sandwich-type Pt-Co-Pt structure.

Another important discovery that we made during our work is that hydrogenation of a graphene layer on a metal substrate does not result in the opening of a band gap. It is generally believed in the graphene community that functionalization of graphene (free standing or supported) through hydrogen adsorption would lead to opening of a band gap either through sub-lattice symmetry breaking or through patterned hydrogenation leading to quantum dot formation.

We show that hydrogenation is accompanied by a symmetry change in the local carbon bonding environment, which causes strong hybridization between the C and Pt atoms. This hybridization leads to pinning of the Fermi level and delocalization of the C π band. Our results shed important light into the possible role played by the substrate in the electronic structure of hydrogenated (or functionalized) graphene, which had not been taken into consideration before. Our work also indicates that it is possible to reversibly form strong local carbon-metal bonds through hydrogenation. This discovery of a possible "welding" method could be important in the design of future graphene devices.

Introduction and Background

Previous studies have indicated that it is possible to approach hydrogen storage capacities of 5-6 wt.% in single walled CNTs (SWNTs) through treatment with an atomic hydrogen source through formation of C–H bonds [1]. However, practical implementation of hydrogen storage in SWNTs requires the development of low-barrier pathways for hydrogen dissociation. One potential pathway could be the "spillover" mechanism, in which molecular hydrogen spontaneously dissociates on a transition metal catalyst attached to the SWNTs, producing mobile H atoms that spill over onto the SWNTs [2]. However, the validity of the spill-over mechanism and the possibility of significant hydrogen storage in SWNTs remain controversial. Only few studies exist including inelastic neutron-scattering (INS) experiments [3] and isotope exchange TPD experiments [4] performed on metal-carbon composites which favorably suggest the existence of a spillover mechanism. Therefore, it is important to obtain a proof of principle for the existence of the spillover mechanism, which could then be exploited for hydrogen storage applications.

Surface science techniques such as temperature programmed desorption (TPD) can provide information about the activation barriers involved in the hydrogen adsorption-desorption process. Since these techniques require well-defined high-quality samples, graphene samples grown on metal substrates at ultra-high vacuum (UHV) conditions were used. Furthermore, another problem of interest to a large community can be studied at the same time, which is the control of the electronic structure through hydrogenation of graphene for electronic applications. Recently, several approaches have been explored to alter the conductance of graphene and substrate-graphene composites through modulation of the electronic structure of graphene [5–8]. While band gap opening through hydrogenation of single layer was reported for graphene/Ir(111) [5] and Au intercalated Ni(111) [8] substrates, it has also been suggested that hydrogenation leads to the formation of mid-gap impurity states for quasi-freestanding graphene [9]. Hence it is important to address the question of whether or not there is a band gap opening resulting from hydrogenation of graphene/metal systems.

The experiments performed on hydrogenated graphene/Pt system indicate that strong grapheme-metal hybridization stabilizes the hydrogenation-induced symmetry change of the local carbon bonding structure. This implies that the hydrogen adsorption-desorption energetics could be controlled through tuning the strength of the resulting hybridization between the graphene overlayer and the metal substrate. Such a tuning could be achieved by modifying the valence *d*-electron structure of the substrate. The *d*-band model [10] describes how chemisorption energies of adsorbates correlate with the average energy of the *d*-electrons with

respect to the Fermi level. The Pt-3*d*-Pt(111) bimetallic sandwich alloys are possible candidates to control ligand environment in the subsurface region, which varies the energy position of the *d*-band center of the topmost layer [11].

Hence we addressed the following sub-tasks in this work:

1. Demonstrate proof-of-principle for the "spillover mechanism" in CNT/Pt composites.
2. Understand the electronic structure changes in graphene/Pt(111) due to hydrogen adsorption.
3. Desorption barrier for hydrogen on graphene/Pt-Co-Pt(111), where a decrease of the H desorption barrier in comparison to graphene/Pt(111) system is expected according to the *d* band model.

Results

Separation and spectroscopy investigations of individual SWNTs (Dai group).

Single-walled carbon nanotubes (SWNTs) are a unique class of macromolecule, conceptualized as a single graphitic sheet of sp^2 carbon atoms, rolled into a seamless cylinder, with diameters of ~ 0.5 – 1.6 nm, and lengths from tens of nanometers up to millimeters. For various applications of nanotubes, it is necessary to obtain individual SWNTs rather than bundled nanotubes, to maximize the surface area for applications such as hydrogen storage and optimize the physical properties of nanotubes such as photoluminescence and resonance raman scattering.

Unfortunately, as-grown SWNTs are heavily bundled. The Dai group set out to obtain purely individual SWNT samples desired for hydrogen storage. We used density gradient centrifugation (DGC) rate (zonal) separation for sodium-cholate suspended SWNTs through an iodixanol step-gradient at ~300,000 g. This method separates nanotubes by mass, with fractions rich in single tubes floating on top of the column and bundles settling at the lower parts of the centrifuge column.

Resonance Raman scattering analysis, under 785 nm laser excitation, of the DGC separated SWNT fractions showed similar intensity trends as the relative photoluminescence (PL) measurements, for both the radial breathing modes (RBMs) and graphitic band (G-band). The DGC separated and absorbance-normalized fractions of SWNTs showed a sharp rise in Raman scattering intensity from fractions 3-6, with a peak in both the RBM and G-band scattering intensity in fraction 6, coinciding with the peak in PL QY. This peak is followed by a gradual decrease in intensity for both modes.

The cause of the gradual loss of both PL QY and Raman scattering intensity in higher fractions is due to presence of small nanotube bundles. Bundling of dispersed SWNTs is known to reduce PL QY via non-radiative energy transfer processes. Excitons can decay non-radiatively into a neighboring metallic nanotube, leading to quenching of the photoluminescence. Bundling also causes red-shifting and absorption peak broadening of the excitonic optical transitions in SWNTs. We observed a red-shift of 13 nm (25 meV) for the optical transition near 800 nm with increasing fraction number. Broadening of optical transition peaks was also observed, suggesting the presence of a broad distribution in the degree of SWNT bundling.

Indeed, Raman scattering analysis revealed an increase in (10,2) RBM intensity indicating an increase in SWNT bundling following DGC, in fraction 7 and above.

The decrease in Raman scattering intensity in higher fractions is related to the red-shifting of the SWNT optical transitions, following from an increasing proportion of SWNT bundles with increasing fraction number. Bundling of SWNTs, perturbs the SWNT single-particle band structure and increases dielectric screening effects, which in turn reduce excitonic optical transitions. This effect is in part mitigated by a decrease in exciton binding energies, but overall the band structure effects outweigh excitonic effects. Charge transfer, caused either by interactions of SWNT sidewalls or the π-density contribution of small aromatic molecules, leads to increased coulomb interactions, and subsequent carrier charge screening, that reduces exciton lifetimes, and leads to PL quenching and contributes to the broadening of optical transitions.

In conclusion, the Dai group has performed density gradient centrifugation (DGC) of sodium cholate-suspended SWNTs in water to separate individual nanotubes from small bundles. Long, individual SWNTs exhibit the highest PL and Raman scattering intensities, 2- to 4-fold higher than as-made SWNT suspensions containing both single and bundled carbon nanotubes. SWNTs found located in high-numbered fractions had higher degrees of bundling, resulting in increasingly red shifted and broadened absorption peaks. This is the first time that a systematic investigation is carried out with separated nanotubes to correlate the photoluminescence, resonance Raman scattering, and optical absorption of individualized versus small, bundled nanotubes. Importantly, our method obtains fractions of highly individualized nanotubes, useful for various applications.

The Dai group has made SWNT film for hydrogen storage studies for this grant. Uniform monolayer of unbundled SWNTs was obtained for the highest loading with Pt and therefore the highest hydrogen-storage capacity on a weight-percent basis. We used individual tubes extracted in this manner to prepare monolayer assemblies of SWNT films by the Langmuir-Blodgett (LB) method, in which SWNTs functionalized by PmPV were dispersed in 1,2-dichloroethane. We calcined the LB films to remove organic solvents, surfactants, and any other remaining contaminants for of Pt coating and hydrogen spill over studies.

In summary, we have performed density gradient centrifugation (DGC) of sodium cholate-suspended SWNTs in water to separate individual nanotubes from small bundles. Long, individual SWNTs are obtained based on spectroscopy measurements. Our method obtains fractions of highly individualized nanotubes, which are now available for hydrogen storage experiments. However, a major next hurdle is to scale up such individual SWNTs to large quantities needed for future realistic storage applications.

Gas phase hydrogen loading - in situ conductivity measurements (Clemens group)

The SWNT samples used were (a) CVD-grown (b) HiPCO samples dispersed employing a combination of nanotube unbundling via density-gradient centrifugation and film deposition using the Langmuir-Blodgett method (LB) and (c) commercial HiPCO samples. The details of the sample preparation are described in our annual report from 2010. The SWNT samples were sputtered with Pt nanoparticles to make Pt-SWNT composites. Pt-SWNT composites with different nominal thickness of sputtered Pt were used in conductivity studies to understand the

influence of catalyst size on hydrogen storage capacity. Details about *in situ* 4-probe resistance measurements under hydrogen gas exposure have been described in our previous annual report.

The resistance measurements were performed under systematic variation of the following parameters: the amount of Pt loading (Fig. 1, 2a), the density of SWNT films (Fig. 2b), and the temperature during hydrogen exposure (Fig. 3).

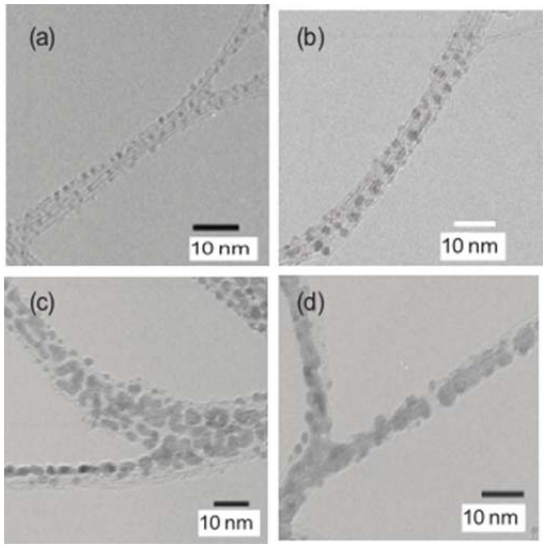

Fig. 1. Evolution of Pt nanoparticle sizes on SWNTs with increasing nominal thickness of deposited Pt (a) 0.2 nm (b) 0.5 nm (c) 1 nm (d) 3 nm.

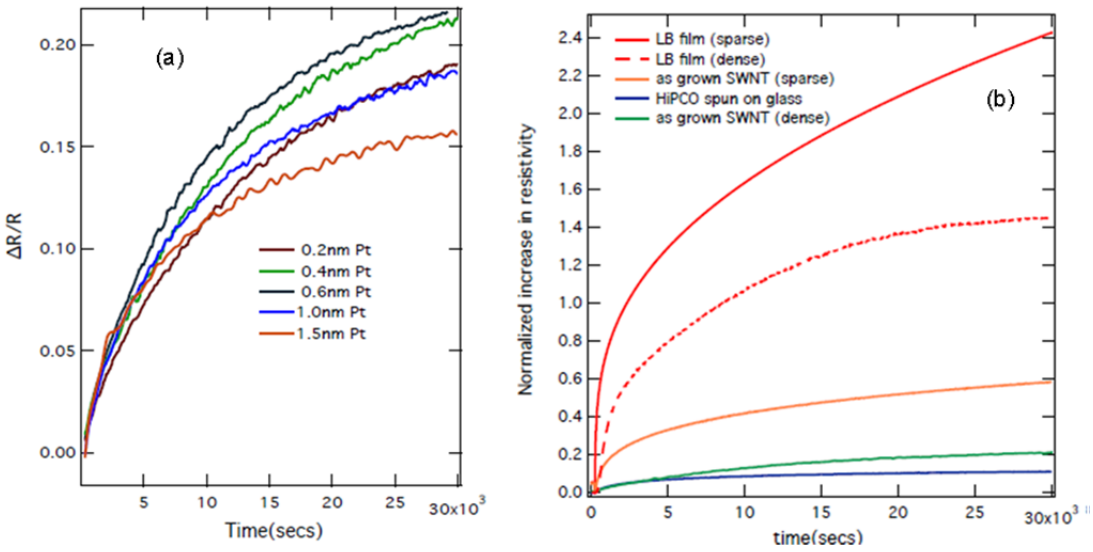

Fig. 2. Normalized resistance change for Pt-SWNTs as a function of exposure time at 700 torr hydrogen gas, (a) using different amounts of deposited Pt (in nominal thickness), (b) using different film preparation techniques resulting in different degrees of SWNT bundling.

TEM micrographs of HiPCO samples with different amounts of deposited Pt are shown in Fig. 1. It could be observed from TEM micrographs that the sputtered Pt film does not wet the SWNT surface but aggregates into particles. The size and distribution of the particles formed depend on the nominal thickness of the sputtered Pt. Increase in nominal thickness of the catalyst particles lead to an increase in normalized resistance to an optimal level, beyond which decrease of normalized resistance was observed (Fig. 2a). The optimal thickness of the deposited Pt film is 0.6 nm (particle diameter ~(2.05 ± 0.36) nm). The TEM micrographs indicate that with an increase in the nominal thickness of the Pt film, the density as well as the size of the catalyst particles increases. Beyond a certain thickness of sputtered film, the Pt particles start agglomerating, thus decreasing the number density of the particles and hence decreasing the extent of possible H spillover onto the SWNT surface. Nominal thickness increase from 0.2 nm to 0.6 nm resulted in an increase in number density of Pt nanoparticles on the SWNTs with slight increase in particle size. Around nominal thickness of 1 nm, reduction in the number density of Pt nanoparticles was observed due to agglomeration of large particles. Hence, the Pt coverage that yields the highest number density of catalyst particles has the highest storage capacity potential. This optimal thickness for maximum hydrogen uptake is in good agreement with hydrogen uptake measurements using a Sieverts apparatus,[5] where it was observed that the hydrogen uptake by a Pt-SWNT composite film varies linearly with the density of the Pt particles.

The effect of SWNT various sample preparation techniques, which result in different degrees of bundling, on the hydrogen uptake is shown in Fig. 2b. Spin-cast films of HiPCO SWNTs and as-grown films produced using CVD show a strong tendency towards formation of bundles; this makes is difficult to efficiently prepare composites with Pt nanoparticles, where direct contact between each nanotube and Pt is desired. Significantly improved hydrogen uptake could be achieved when we used a CVD procedure that yielded less dense films. The greatest improvement so far has been found with a procedure where unbundled HiPCO SNWTs were isolated using density gradient centrifugation, and subsequently deposited using the Langmuir-Blodgett technique.

It was observed that the resistance plots do not saturate during the time scale of the hydrogenation experiments (8 hours), indicating slow kinetics. We conjecture that diffusion of H over the SWNT surface is rate-limiting in the hydrogenation mechanism. In fact, we found that increasing the temperature increases the initial hydrogen uptake rate and, at temperatures higher than 94 °C, equilibrium can be reached during the timescale of our experiment. On the other hand, the overall change in resistance at any time beyond ~2 h is the largest at -5 °C and decreases monotonically with increasing temperature. Hence, while increased temperatures improve the kinetics of the hydrogen spillover, at the same time the thermodynamic equilibrium is unfavorably shifted, decreasing the hydrogen storage capacity.

(a) **(b)**

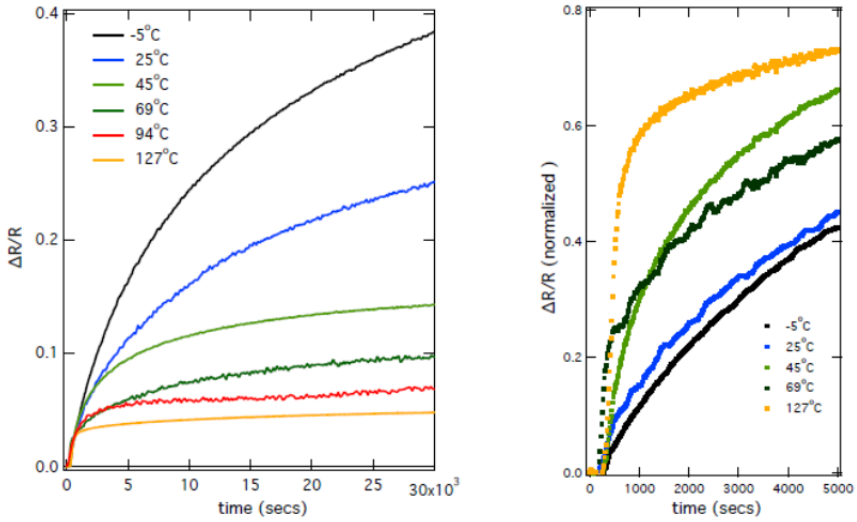

Fig. 3. (a) Hydrogen uptake measured at different temperatures, (b) enlarged plot showing the initial behavior.

Direct evidence for C–H bond formation in carbon nanotubes: XPS studies (Nilsson group)

In order to verify that the changes observed in conductance measurements are indeed due to hydrogenation, XPS measurements of CVD-grown (CVD) and LB-film samples with a nominal 0.6nm thickness of deposited Pt were performed before and after hydrogen exposure (8.27 bar H_2 at room temperature for 3 hours). The incident x-ray energy was set to $h\nu_{in}$ = 400 eV. The C 1s spectra are shown in Fig. 4 and Fig. 5, with the binding energy referenced to the Fermi level. The full-width at half-maximum (FWHM) of the C 1*s* peak before hydrogen loading is 1.4 and 1.15 eV for the CVD-grown SWNTs (Fig. 4a) and LB films (Fig. 5a), respectively. For both the CVD-grown and LB-film composites, the spectra acquired before hydrogen exposure can be fitted with a single asymmetric Gaussian-Lorentzian (GL) component centered at 284.8 eV (Fig. 4b and 5b), corresponding with sp^2-hybridization of the C atoms; the asymmetric tail of these spectra can be attributed to electron-hole pair excitations at the Fermi level arising from the metallic nature of the CNTs. After exposure to hydrogen at a pressure of 8.27 bar for 6 hours, the FWHM of the C 1*s* spectrum of the CVD-grown SWNTs increased to 1.5 eV (Fig. 4(a)), while that of the LB films increased to 1.35 eV (Fig. 5(a)). Peak fitting reveals a new feature in addition to the previously observed sp^2-peak, which we fitted using a symmetric GL with 2 eV FWHM. This new spectral contribution is assigned to C atoms that have undergone rehybridization from sp^2 to sp^3 due to the breaking of C–C π-bonds and C–H bond formation,[1] and can be seen as a direct evidence for the proposed spillover effect.

An additional peak at 288 eV (shifted by ~3.3 eV from the main sp^2 C1s peak) can be detected for hydrogenated samples. A similar feature was observed when pure SWNTs were treated with atomic hydrogen.[6] We conjecture that this additional peak arises from a metal-to-semiconductor transition of the nanotubes that is induced by hydrogenation. The decrease in conductivity accompanying such a transition can cause a reduction of the core-hole screening that increases the final-state energy by ~2-3 eV. The hydrogen uptake due to exposure to molecular hydrogen of ~8.27 bar, quantified by XPS indicates 1.2 wt.% hydrogen storage for LB-film composites and 1 wt.% for CVD-grown CVD composites.

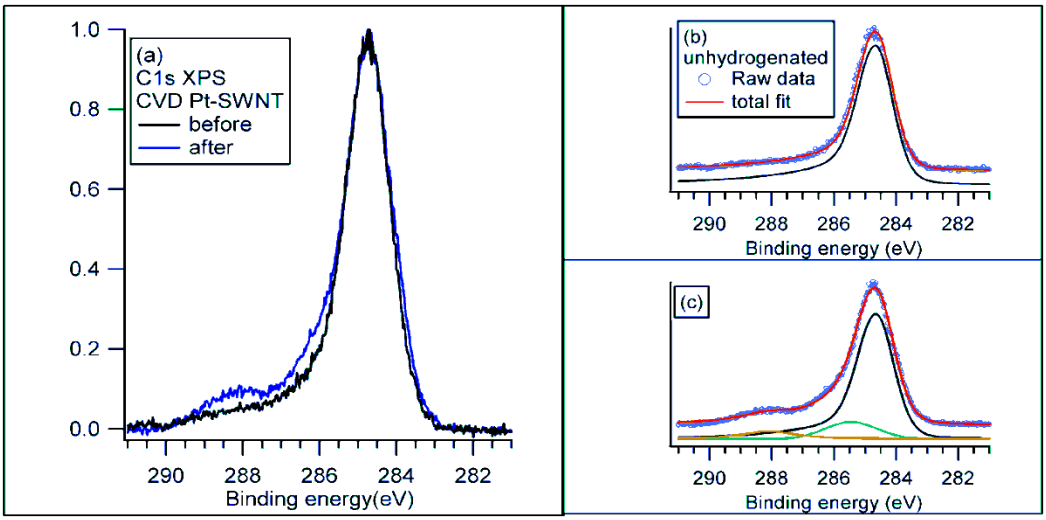

Fig 4. (a) C 1*s* XPS spectra before (*black*) and after (*blue*) hydrogen charging for CVD-grown film with 0.6nm Pt; the spectra are normalized to peak maxim to enhance differences in the peak shapes. Gaussian-Lorentzian deconvolution (see text for details) **(b)** before and **(c)** after hydrogen charging: raw data (*open blue circles*); total fit (*red*); sp^2-C peak (*black*); sp^3-C peak (*green*); additional peak due to hydrogen-induced metal-to-semiconductor transition (*orange*). Fits are offset from raw data for clarity.

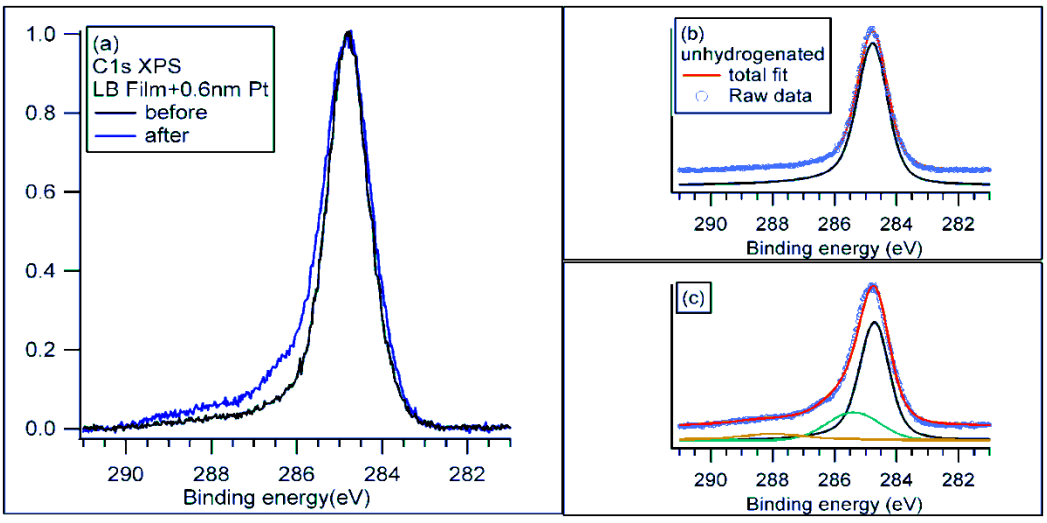

Fig. 5. (a) C 1*s* XPS spectra before and after hydrogen exposure for an LB film with 0.6nm Pt; the peak maxima of both spectra are normalized to enhance differences in the peak shapes. Gaussian-Lorentzian deconvolution (see text for details) **(b)** before and **(c)** after hydrogen charging: raw data (*open blue circles*); total fit (*red*); sp^2-C peak (*black*); sp^3-C peak (*green*); additional peak due to hydrogen-induced metal-to-semiconductor transition (*orange*). Fits are offset from raw data for clarity.

Probing hydrogengenation in graphene on Pt (Nilsson group)

In order to complement the work performed on the carbon nanotubes with more well defined surfaces we have conducted studies of hydrogenation of graphene on Pt surfaces. Graphene layers on Pt(111) were prepared under UHV conditions by cracking ethylene. Our studies on growth and electronic structure of grapheme/Pt(111) have been published in Ref [13]. The most important finding from this study is that the graphene growth was accompanied by Moiré rippling and the overlayer was very weakly interacting with the Pt(111). The interaction could be thought of as a charge doping.

The graphene samples were hydrogenated using a commercial atomic hydrogen source (Omicron). We briefly discuss hydrogenation-induced geometric structure changes. Fig. 1(a) shows a scanning tunneling microscopy (STM) image of graphene domains, which exhibit a characteristic superstructure lattice with a periodicity of 1.95 nm, which has been characterized as the $\sqrt{63}\times\sqrt{63}\,\mathrm{R19}$ structure in a previous study by Enachescu et al. [14]. Bright and dark regions of the honeycombs indicate out-of-plane rippling of graphene as well as varying registry of the carbon atoms with respect to Pt surface atoms. The morphology of graphene after hydrogenation is shown in Fig. 1(b). Ring-like structures were observed on top of the periodic structure of graphene. Most rings delocalized around the bright honeycombs of graphene while some coalesce to form elongated bright structures. Nonetheless, a Fourier transform of the STM image (inset of Fig. 1(b)) shows that the superstructure remains intact, in agreement with a previous study on the hydrogenation of graphene on Ir(111) [5]. The C 1*s* XP spectra of graphene and hydrogenated graphene are shown in Fig. 1(c). C 1*s* spectra for graphene on Pt(111) exhibit a narrow line width consisting of a single component corresponding to sp^2 hybridized carbon atoms. The two most important features of hydrogenation are the formation of C-H bonds and an increased C-Pt hybridization. We observe a C-H component at ~284.8 eV [15], a lower BE shoulder (~283.7 eV) due to defects, and a component which corresponds to C-Pt hybridization (~284.3 eV). Features observed in Pt $4f_{7/2}$ peak (Fig. 1(e)) directly manifest this C-Pt hybridization. The mutual decay of the Pt surface state and appearance of a higher BE shoulder at 71.4 eV, corresponds to the increased graphene-Pt interaction. This interaction is likely due to the overlap between the valence states of Pt and carbon. The deconvolution of C 1*s* XP spectra of hydrogenated graphene reveals the sp^2 (22%), C-H (42%), defect (10%) and C-Pt hybridized (26%) components. The spectral weights are consistent with the observed maximum deuterium coverage determined with TPD measurements (0.42 ML) and with the disappearance of the surface component in the Pt $4f_{7/2}$ spectrum.

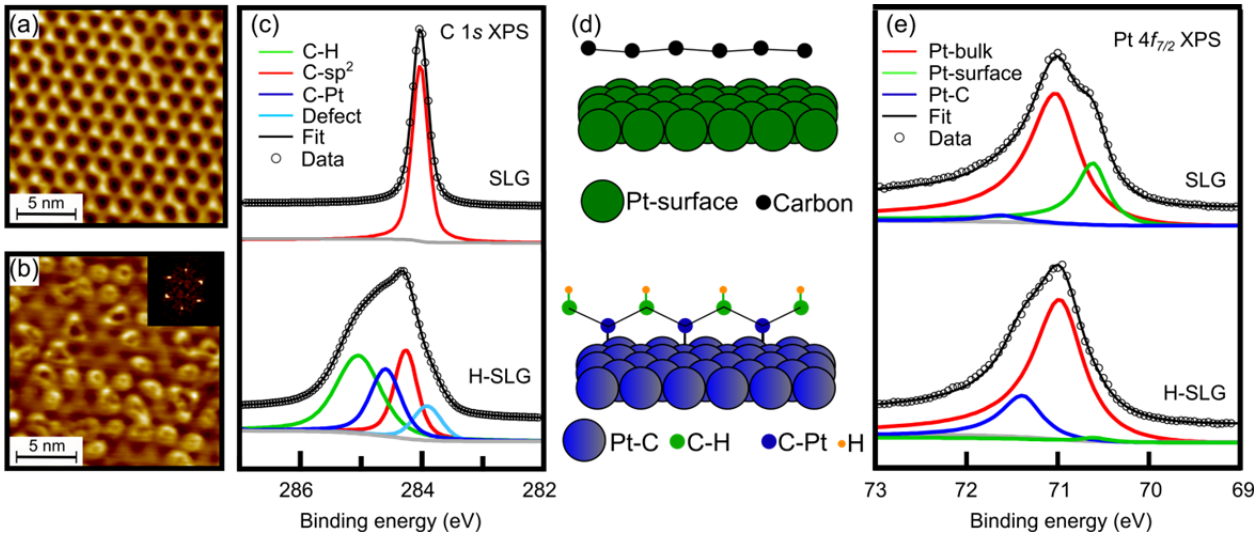

Figure 1- STM images of (a) graphene (SLG) and (b) hydrogenated graphene (H-SLG). Inset of (b): Fourier transform of STM image of H-SLG. (c) C 1*s* XPS ($h\upsilon_{in}$ = 400 eV) of SLG (top) and 0.42 ML H-SLG (bottom) (d) Sketches of pinning of carbon atoms to the Pt surface atoms after hydrogenation at the bright parts of the Moire pattern (top – SLG on Pt(111), bottom – H-SLG on Pt(111)). (e) Pt $4f_{7/2}$ XPS ($h\upsilon_{in}$ =165 eV) of SLG (top) and H-SLG (bottom). The spectra were deconvoluted using Gaussian-broadened Doniach-Šunjić functions. Assignments of C-Pt, C-sp^2,C-H, and defect components are made based on Pt $4f_{7/2}$ XPS, XAS (see below) and TPD measurements.

The dipole selection rule and polarization-dependence in XAS and XES are utilized to map symmetry-resolved σ and π chemical bonding [16]. Since both excitation and de-excitation processes involve the 1s core-hole state localized on the core-excited C atom, the spectra are interpreted in terms of the C 2*p* partial density of states (DOS) in the carbon layer. Thus, carbon-metal bonding contributions are extracted and clearly separated from the overall band structure. C K-edge XAS selectively probes the 2*p*-projected unoccupied DOS (u-DOS, conduction band) while XES measures the occupied DOS (o-DOS, valence band). The 2*p*-projected carbon DOS of graphene obtained by XES and XAS is shown in Fig. 2. It is clear that there is no band gap opening (i.e. there is still finite DOS at Fermi level after hydrogenation).

Our findings on hydrogenation of graphene/Pt(111) can be summarized as follows: hydrogenation modifies the structure of graphene as described in Fig. 1, which results in strong hybridization of the carbon atoms with Pt substrate atoms. Hence, the hydrogenated graphene structure is stabilized through this C-Pt hybridization. As a consequence of the latter, there is no band gap opening in hydrogenated graphene.

Based on the previous work, it is expected that modification of the strength of C-Pt hybridization would change the energetics of (de-)hydrogenation. Reduction of the activation barrier for hydrogenation could have an effect on hydrogen storage applications and novel

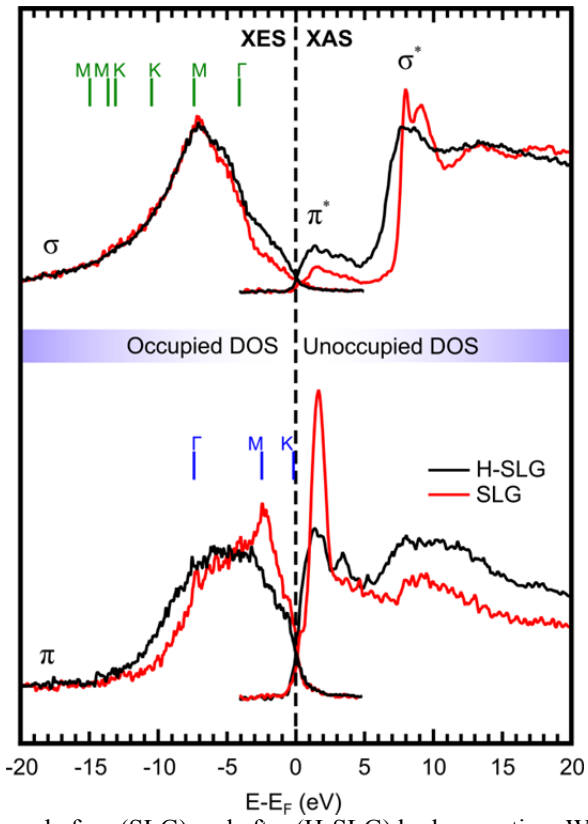

Figure 2- Measured DOS of graphene before (SLG) and after (H-SLG) hydrogenation. We could observe that there is still finite DOS in H-SLG which is attributed to C-Pt hybridization as elucidated in Fig 1.

electronic device manufacturing. In order to achieve this, samples of the form graphene/Pt-Co-Pt(111) were prepared. Graphene was first grown on Pt(111) as described above, and then Co was evaporated at 600K. At this temperature, Co atoms can overcome diffusion barriers and migrate to subsurface sites, thus forming the Pt-Co-Pt sandwich-type structure which is thermodynamically favored over an exposed Co layer due to its high surface energy. The subsurface intercalation of Co has been confirmed with various surface science techniques (not discussed in this report).

TPD was used to observe the desorption temperature of hydrogen from the graphene layer. A comparison of TPD between graphene/Pt(111) and graphene/Pt-Co-Pt(111) is displayed in Fig 3. There is a significant shift of the desorption peak towards lower temperatures hence validating our assumption that the desorption barrier can be controlled by modification of the electronic states of the metal.

It has been shown that annealing Pt-Co-Pt(111) samples to temperatures around 1000 K drives all the Co atoms into the bulk, resulting in almost infinite dilution of the Co content and thus a surface behavior almost identical to Pt(111). Hence, the desorption behavior of hydrogen, for Pt-Co-Pt(111) samples annealed to 1000 K, should be similar to that of graphene/Pt(111). We indeed observe this occurrence in Fig 3.

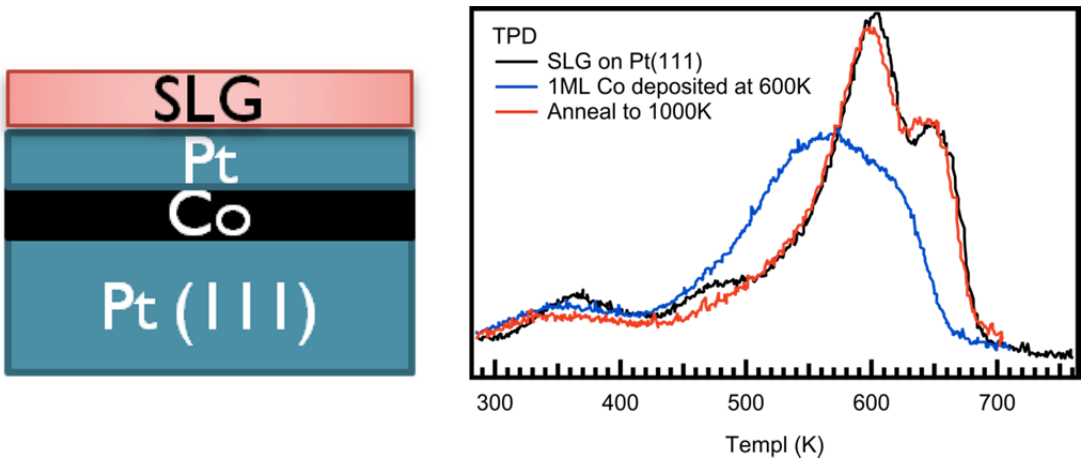

Figure 3 – (Left) Schematic of graphene (SLG) on Pt-Co-Pt(111). (Right) Hydrogen TPD from hydrogenated graphene layer. The shift in desorption towards lower temperatures is clearly observed for SLG/Pt-Co-Pt(111).

Conclusion

The results of our work can be summarized in three key achievements:

1. The spillover mechanism could be utilized for hydrogenating carbon nanostructures at near ambient conditions. We achieved up to 1.6 wt.% of hydrogen storage in CNT/Pt composites.
2. We have identified the electronic structure modification induced by hydrogenation of graphene on metal substrates. Strong carbon-metal hybridization prevents the formation of a bandgap. Hydrogen-induced carbon-metal bonding could be used for "spot-welding" of nanometer-sized contacts in graphene-based electronic devices.
3. The desorption energetics of hydrogen on graphene samples on metal substrates can be tuned through modification of the electronic structure of the underlying substrate.

The results demonstrate that hydrogen storage in carbon nanotubes could be viable way forward using a catalyst. The challenge is that the production of carbon nanotubes with well defined properties is still most difficult. We can tune the metal interaction with carbon composite in order to obtain the right C-H bond strength.

Publications

1. S. M. Tabakman, K. Welsher,† G. Hong, and H. Dai, Optical Properties of Single-Walled Carbon Nanotubes Separated in a Density Gradient:Length, Bundling, and Aromatic Stacking Effects, J. Phys. Chem. C **114**, 19569–19575 (2010).
2. R. Bhowmick, S. Rajasekaran, D. Friebel, C. Beasley, L. Jiao, H. Ogasawara, H. Dai, B. Clemens, and A. Nilsson, Hydrogen Spillover in Pt-Single-Walled Carbon Nanotube Composites: Formation of Stable C_H Bonds J..Am. Chem. Soc. **133**, 5580–5586 (2011).
3. S. Rajasekaran, S. Kaya, T. Anniyev, H. Ogasawara, and A. Nilsson, Probing substrate effects in the carbon-projected band structure of graphene on Pt(111) through resonant inelastic x-ray scattering**,** Phys. Rev. B **85**, 045419 (2012).

4. S. Rajasekaran, S. Kaya, Frank Abild-Pederson, T. Anniyev, F. Yang, D. Stacchiola, H. Ogasawara, and A. Nilsson, Reversible Graphene Metal Contact through Hydrogenation (submitted, 2012).
5. S. Diao, G. Hong, J. Robinson, A. Antaris, Single chirality enriched (12,1) single walled carbon nanotubes by gel fitration method (submitted 2012).

References

[1] A. C. Dillon, K. M. Jones, T. A. Bekkedahl, C. H. Kiang, D. S. Bethune, and M. J. Heben, Nature **386**, 377–379 (1997).
[2] G. A. Somorjai, *Introduction to Surface Chemistry and Catalysis* (Wiley, 1994).
[3] P. C. H. Mitchell, A. J. Ramirez-Cuesta, S. F. Parker, J. Tomkinson, and D. Thompsett, The Journal of Physical Chemistry B **107**, 6838–6845 (2003).
[4] A. J. Lachawiec Jr and R. T. Yang, Langmuir **24**, 6159–6165 (2008).
[5] R. Balog, B. Jorgensen, L. Nilsson, M. Andersen, E. Rienks, M. Bianchi, M. Fanetti, E. Laegsgaard, A. Baraldi, S. Lizzit, Z. Sljivancanin, F. Besenbacher, B. Hammer, T. G. Pedersen, P. Hofmann, and L. Hornekær, Nat. Mater. **9**, 315–319 (2010).
[6] A. Bostwick, J. L. McChesney, K. V. Emtsev, T. Seyller, K. Horn, S. D. Kevan, and E. Rotenberg, Phys. Rev. Lett. **103**, 056404 (2009).
[7] D. C. Elias, R. R. Nair, T. M. G. Mohiuddin, S. V. Morozov, P. Blake, M. P. Halsall, A. C. Ferrari, D. W. Boukhvalov, M. I. Katsnelson, A. K. Geim, and K. S. Novoselov, Science **323**, 610 –613 (2009).
[8] D. Haberer, D. V. Vyalikh, S. Taioli, B. Dora, M. Farjam, J. Fink, D. Marchenko, T. Pichler, K. Ziegler, S. Simonucci, M. S. Dresselhaus, M. Knupfer, B. Büchner, and A. Grüneis, Nano Lett. **10**, 3360–3366 (2010).
[9] D. Haberer, L. Petaccia, M. Farjam, S. Taioli, S. A. Jafari, A. Nefedov, W. Zhang, L. Calliari, G. Scarduelli, B. Dora, D. V. Vyalikh, T. Pichler, C. Wöll, D. Alfè, S. Simonucci, M. S. Dresselhaus, M. Knupfer, B. Büchner, and A. Grüneis, Phys. Rev. B **83**, 165433 (2011).
[10] B. Hammer and J. K. Norskov, Nature **376**, 238–240 (1995).
[11] J. R. Kitchin, J. K. Nørskov, M. A. Barteau, and J. G. Chen, J. Chem. Phys. **120**, 10240–10246 (2004).
[12] R. Bhowmick, S. Rajasekaran, D. Friebel, C. Beasley, L. Jiao, H. Ogasawara, H. Dai, B. Clemens, and A. Nilsson, J. Am. Chem. Soc. **133**, 5580–5586 (2011).
[13] S. Rajasekaran, S. Kaya, T. Anniyev, H. Ogasawara, and A. Nilsson, Phys. Rev. B **85**, 045419 (2012).
[14] M. Enachescu, D. Schleef, D. F. Ogletree, and M. Salmeron, Phys. Rev. B **60**, 16913 (1999).
[15] A. Nikitin, L.-A. Näslund, Z. Zhang, and A. Nilsson, Surf. Sci. **602**, 2575–2580 (2008).
[16] A. Nilsson and L. G. M. Pettersson, Surf. Sci. Rep. **55**, 49–167 (2004).

Contacts

Anders Nilsson: nilsson@slac.stanford.edu

Hongjie Dai: hdai1@stanford.edu

Bruce Clemens: bmc@stanford.edu